

Developing a Generalized Model for Compartmentalization of Organometallic Catalysis

Brandon J. Jolly¹, Chong Liu^{1,2*}

¹Department of Chemistry and Biochemistry, University of California, Los Angeles, California
90095, United States

²California NanoSystems Institute (CNSI), University of California, Los Angeles, Los Angeles,
CA 90095, USA

† Equal contributions of authorship

* To whom correspondence may be addressed. Email: chongliu@chem.ucla.edu

Abstract: Compartments can improve the efficiency of cascade reactions through retainment of ephemeral intermediates by minimizing competing elimination pathways. Numerous examples of compartments exist in biocatalysis, one such example being oxygen sensitive nitrogenases in microbes, where the enzyme is spatially located in an anaerobic domain to prevent deactivation. Recently, extensive efforts have been devoted to developing models and guiding design principles for compartmentalization of biocatalytic cascades. However, little to no effort has been devoted to analyzing compartmentalization of organometallic catalytic cycles from a theoretical perspective, which reasonably may benefit from compartmentalization given their numerous, common deactivation pathways. Herein, we develop a mathematical model for compartmentalization of a general three step organometallic catalytic cycle operating within a nanowire array electrode as an example nanostructure. Under the same kinetic parameters, the model predicts that compartmentalization enhances key reaction metrics, being intermediate elimination/outflux, reaction conversion, and turnover frequency in comparison to a non-compartmentalized cycle. We show that tuning mass transport through variation of nanostructure geometry is a viable approach to optimizing the turnover of a solution cascade reaction. Furthermore, we demonstrate that elimination reactions occurring outside of the compartment establish a concentration gradient that with feasible diffusive conductance, augments intermediate outflux. We posit that a well designed nanostructure will circumvent this issue even with fast eliminations. The model serves as a starting point and may be adapted to suit any organometallic catalytic cycle and nanostructure geometry.

INTRODUCTION

Biology has long utilized compartmentalization to protect enzymes from deactivation environments, as well as retain reactive intermediates in cascade reactions. (Refs) The field of biocatalysis has extensively studied ways to experimentally exploit this idea to improve tandem or cascade enzymatic transformations.¹⁻³ In order to mimic biological compartments, several groups have developed nano/micro confinement's such as lipid micro droplets and MOF's to operate biocatalytic cascades in.⁴ Following these efforts, several groups, such as Tsitkov et al., have generated guiding design principles for such compartments through mathematical modeling of fundamental kinetic and diffusive steps.⁵⁻⁸ A key takeaway of these efforts is the careful tuning of diffusive conductance, F , which is defined as the product of compartment permeability (p), surface area (SA), and Avogadro's number (N_A).⁸ Though significant progress has been made with respect

to biocatalysis, little effort has been devoted to explore the concept of compartmentalization in organometallics.

Our group previously employed a nanowire array electrode to generate a catalytic cycle of incompatible steps consisting of rhodium metalloporphyrin (RhPor) mediated CH₄ activation, and O₂ mediated methanol formation.^{9,10} Even though the cycle proceeds through an oxygen sensitive Rh(II) intermediate, the creation of a local oxygen gradient by applying a reducing potential to the nanowire array electrode enabled this cycle to proceed efficiently under ambient conditions. The retainment of the ephemeral Rh(II) intermediate to ensure subsequent CH₃OH formation led us to further analyze this system in the context of a compartmentalized cascade. In a follow up report, we developed a mathematical model of the RhPor CH₄ activation operating under ambient conditions in a nanowire array electrode and solved for key reaction metrics such as efficiency (γ), defined as product formation (R_p) divided by substrate consumption (R_s).¹¹ By adapting the definition of F for the geometry of a nanowire, we showed that experimentally derived γ closely matches the model, suggesting that the cycle proceeds efficiently as a compartmentalized system. Furthermore, the model shows that optimization is possible by controlling mass transport through the tuning of F , which is a function of nanowire geometry.

The development of diverse nanostructures, including nanowires, offers a novel path to explore the heterogeneous – homogeneous interface. In addition, nanostructures as we have previously shown, are a viable approach to compartmentalizing organometallic reactions, especially electrochemically mediated ones. We envision that the concept of compartmentalization by means of nanostructures can be generally applied to benefit organometallic catalysis, as a plethora of transition metal based catalysts are oxygen sensitive. Furthermore, several organometallic mediated transformations are net oxidative, thus it would be cost effective and sustainable to utilize O₂. Our approach to illustrating this concept is to develop a mathematical model for a compartmentalized general catalytic cycle (Fig 1) based on fundamental kinetic and diffusive steps that is more in depth and broadly applicable than our previous one. Through solving for key reaction metrics such as efficiency (γ), intermediate outflux/elimination (R_i), and turnover frequency (TOF), we show that under the same parameters, a compartmentalized system outperforms a homogeneous counterpart from a theoretical perspective. In addition, we further support that optimization is possible through tuning F , which serves as a guiding design principle. Elimination rate constants (k_{en}) impose a secondary effect on a compartmentalized system by

establishing an external concentration gradient where outflux is then a function of F , suggesting that deactivation pathways should still be strongly considered when a proper compartment is designed. We restrict our model to a nanowire geometry, but discuss how other nanostructures may be accounted for. The model may be easily adapted to suit any catalytic cycle or nanowire geometry, offering a framework to expand on and utilized to design compartmentalized organometallic cycles within nanostructures.

RESULTS AND DISCUSSION

Compartmentalized framework for a general catalytic cycle

Following our previous work with employing a nanowire array electrode to develop a solution catalytic cycle of incompatible steps and subsequent work showing it may be regarded as a compartmentalized system, we set out to demonstrate that compartmentalizing organometallic catalytic cycles is generally beneficial by means of nanostructures.^{10,11} We chose to model a general three step catalytic cycle (Fig 1A) in the context of a compartmentalized system. Furthermore, we elected to use a nanowire array as an example nanostructure given our previous experience utilizing them. Within the model, a catalytic species, Cat, may diffuse into the compartment barring any elimination and bind substrate molecule A through oxidative addition to form intermediate species Cat-A, either first or second order with respect to Cat ($m = 1, 2$). Diffusion of Cat into the compartment, governed by diffusive term F_V , is in direct competition with elimination, governed by k_{e1} , which may be omitted if no elimination is known. Once Cat-A is generated, it may convert product adduct species Cat-B through isomerization or migratory insertion, governed by k_2 . This step is in direct competition with outflux of Cat-A to the bulk solution, governed by F_V and elimination, governed by k_{e2} . Cat-B may then give off product B through reductive elimination and regenerate Cat, governed by k_3 . This process is also in competition with diffusion out of the compartment and be eliminated, governed by F_V and k_{e3} respectively.

Next, we expanded on our previous definition of F_V , where $F_V = F/VN_A$ and F is diffusive conductance in $M s^{-1}$.⁸ In brief, F is defined as the product of compartment permeability (p), surface area (SA), and Avogadro's number (N_A). However, in order to obtain the flux of a particular species, F is normalized to the volume of the compartment (V) and N_A . We suspect that F and V will be interrelated, so we introduced term F_V to generate an expression for F/VN_A . Terms such

as p and V may be solved for in terms of nanostructure geometry, which in the nanowire case will be wire length L (ranging from 10 – 50 μm).¹⁰ Previously, we obtained the following expression

$$F_V = \frac{8D}{L^2} \quad (1)$$

where D is the diffusion coefficient of a catalytic species. However, one limitation of this expression is that probability of diffusion of a molecule at any point along the wire is assumed to be equal. We postulate that diffusion out of the array near the tip is far more feasible than at the base of the wire. Therefore, we took an integral weighted average of our previous definition of F_V at incremental wire lengths. For a more in depth explanation of the F_V derivation, see Supplementary Information Section 1A.

$$F_V = \frac{\int_L^0 F_V w(L) dL}{\int_L^0 w(L) dL} \quad (2)$$

$$\text{where } w(L) = L$$

To simplify the model, we make a few assumptions. As a first order approximation, substrate and product molecules A and B are assumed to be relatively small with respect to the catalytic species, therefore D does not change significantly throughout the cycle and F_V only varies with L . In addition, for elimination reactions to be considered, their rate constants (k_{en}) must be on par with the rate constant (k_{n}) of steps they are in competition with. Thus, we approximated that $k_{\text{n}} = k_{\text{en}}$, unless otherwise stated. We also assume that product release from Cat-B species proceeds relatively fast ($k_3 = 1 \times 10^6 \text{ s}^{-1}$), therefore we do not explore the effect of varying k_3 or k_{e3} on the model. Diffusion coefficient is averaged to be $9 \times 10^{-10} \text{ cm}^2 \text{ s}^{-1}$, based off a range of literature diffusion coefficient values for organometallic catalysts.^{12,13} A range of rate constants for k_1 and k_2 were gathered from literature.^{9,10,14-21} Lastly, we assume steady state of catalytic species within the compartment and in bulk. The rates of catalytic species in the compartmentalized framework are as follows:

$$\frac{d[\text{Cat}]}{dt} = F_V(C_{\text{Cat},\text{total}} - [\text{Cat}]) + k_3[\text{Cat} - \text{B}] - k_1[\text{Cat}]^m C_A - k_{e1}(C_{\text{Cat},\text{total}} - [\text{Cat}]) \quad (3)$$

$$\frac{d[\text{Cat} - \text{A}]}{dt} = -F_V([\text{Cat} - \text{A}] - [\text{Cat} - \text{A}]_b) + k_1[\text{Cat}]^m C_A - k_2[\text{Cat} - \text{A}] - k_{e2}[\text{Cat} - \text{A}] \quad (4)$$

$$\frac{d[\text{Cat} - \text{A}]_b}{dt} = F_V([\text{Cat} - \text{A}] - [\text{Cat} - \text{A}]_b) - k_{e2}[\text{Cat} - \text{A}] \quad (5)$$

$$\frac{d[Cat - B]}{dt} = -F_V([Cat - B] - [Cat - B]_b) + k_2[Cat - A] - k_3[Cat - B] - k_{e3}[Cat - B] \quad (6)$$

$$\frac{d[Cat - B]_b}{dt} = F_V([Cat - B] - [Cat - B]_b) - k_{e3}[Cat - B] \quad (7)$$

Here, $C_{Cat,total}$ is the total concentration of the initial catalytic species from the bulk solution; C_A is the concentration of substrate A from the bulk solution; $[Cat]$, $[Cat - A]$, and $[Cat - B]$ are the steady state concentrations of the three catalytic species within the compartment; $[Cat - A]_b$ and $[Cat - B]_b$ are the steady state concentrations of Cat-A and Cat-B in the bulk that arise from outflux. A non-compartmentalized framework was also generated by dropping diffusive terms and redefining intermediate outflux as intermediate elimination (Supplementary Information Section 2). All key reaction metrics are listed in Figure 1B, namely reaction efficiency (γ), intermediate outflux (R_I), and turnover frequency (TOF). By solving for the steady state concentration of catalytic species, the following expressions are obtained in the context of a compartmentalized system when $m = 1$:

$$\gamma = \frac{k_2 k_3}{(f_2 + k_2)(f_3 + k_3)} \quad (8)$$

$$R_{P3,m=1} = \frac{k_1 k_2 k_3 C_{Cat,total} [A] (F_V - k_{e1})}{(a_1 + F_V - k_{e1})(f_2 + k_2)(f_3 + k_3)} \quad (9)$$

$$TOF_{3,m=1} = \frac{k_1 k_2 k_3 C_A (F_V - k_{e1})}{(a_1 + F_V - k_{e1})(f_2 + k_2)(f_3 + k_3)} \quad (10)$$

The term a_1 is an abbreviation of several kinetic parameters that appeared in the derivation often, and is utilized for simplicity. Its full expression can be found in Supplementary Information __. The full derivation, as well as expressions for the $m = 2$ and the non-compartmentalized system can be found in Supplementary Information __, though we note that γ was derived not to depend on reaction order, as it is a ratio between R_P and R_S . We refrain from explicitly defining turnover number (TON) as there are numerous system dependent definitions, and it would be difficult to express turnovers until catalyst deactivation within the confines of a numerical model. However, we hypothesize that TON will exhibit similar parameter dependencies as TOF. Since retainment of reactive intermediates is a key function of compartments, we focus our discussion on the effect of k_2 and k_{e2} on reaction metrics.

Comparing Compartmentalized Performance to Non-Compartmentalized

In order to assess retainment of the intermediate species Cat-A, we first explored the effect k_2 and F_V had on the compartmentalized system by plotting γ , R_I , and TOF as a function of those two variables. Figure 2A shows that k_2 can effectively outcompete F_V in a compartmentalized system to approach an efficiency near unity. Furthermore, the compartmentalized system achieves nearly twice the efficiency of a non-compartmentalized counterpart under identical kinetic parameters using a 15 μm nanowire with $F_V = 320 \text{ s}^{-1}$ (Fig 2B). From a nanostructure design perspective, Figure 2B shows little to no difference when $k_2 \ll F_V$. However, once k_2 approaches the value of F_V , the compartmentalized system significantly out-performs the non-compartmentalized. Thus, if the value of k_2 is known, a nanostructure should be crafted to produce an F_V value near or less than k_2 .

The results of Figure 2 are further corroborated by exploring R_I as a function of k_2 and F_V . Shown in Figure 3A, R_I significantly decreased with increasing k_2 , spanning a four order of magnitude decrease in intermediate outflux when $m = 1$. In addition, R_I intuitively increases with F_V , albeit minimal on log scale in the range of nanowire lengths explored. A similar trend is observed for R_I when $m = 2$ (Supplementary Fig 5A). Dependence on F_V will be discussed further in a later section. A similar result to that obtained in Figure 2B is seen in Figure 3B. When $k_2 \ll F_V$, the compartmentalized system has approximately the same intermediate outflux/elimination as the non-compartmentalized system. However, as k_2 approaches F_V and becomes larger, the compartmentalized system has between one to two order of magnitudes lower intermediate outflux/elimination. This further supports the careful design of nanostructure geometry in relation to kinetic parameters, and is also what explains higher efficiency in the compartmentalized system.

Lastly, the effects of k_2 and F_V on TOF can be seen in Figure 4. In Figure 4A, the model predicts that TOF is proportional to k_2 , and inverse to F_V , due to increased intermediate outflux. Though it should be noted that relatively low TOF values are predicted, most likely due to k_1 being set at 0.1 M s^{-1} for the $m = 1$ case, as well as the approximation that $k_n = k_{en}$. A similar trend is observed for TOF when $m = 2$ (Supplementary Figure 6A). Figure 4B shows that the compartmentalized system outcompetes the non-compartmentalized in terms of TOF at all k_2 values using the same 15 μm wire .

Nanostructure Design Insight from Dependences on F_V and k_{en}

In order to get a clearer picture of the effect of nanostructure geometry on mass transport and subsequently key reaction metrics, γ , R_I , and TOF are displayed as a function of F_V in Figure 5. γ and TOF are shown to be inversely proportional to F_V when all other variables are held constant, and R_I intuitively is proportional to F_V . These results further support the ability to tune and optimize the system by tuning nanostructure geometry. It should be noted that the model suggests that a lower F_V value, which equates to a longer wire in the nanowire example, is ideal. However, we postulate that experimentally, too small of an F_V value will hinder Cat-A outflux, but would also slow down Cat influx, possibly to the point where efficiency and TOF would decrease. Traces for R_I and TOF when $m = 2$ are also displayed in Figure 5B and 5C (black trace), respectively. The overall trends are similar to the $m = 1$ case, presumably because $[Cat]$ is unchanged, with the only difference being the magnitude of R_I and TOF, due to differences in k_1 for $m = 1$ ($0.1 \text{ M}^{-1} \text{ s}^{-1}$) and $m = 2$ ($10 \text{ M}^{-2} \text{ s}^{-1}$) based on literature reports discussed earlier. Interestingly, TOF does not decrease significantly in the range of F_V values explored here relative to R_I and γ . This suggests that as long as a cascade reaction is adequately compartmentalized, turnovers are ensured to occur.

Even though elimination reactions are assumed to occur solely outside the compartment, it is probably that they still indirectly affect a cascade reaction occurring inside a compartment. Figure 6 displays γ and R_I as a function of F_V and k_{e2} and predicts minimal decrease in γ even with a large k_{e2} value when F_V is sufficiently small. As F_V increases, a significant concomitant decrease in γ is observed with high k_{e2} . One interpretation of this result is that k_{e2} (or k_{en} in general) serves to establish a concentration gradient of $Cat - A$ directed outside of the compartment. With minimal diffusive conductance, $Cat - A$ does not feasibly outflux and efficiency is maintained relatively high. However, once F_V increases, $Cat - A$ becomes more probable and efficiency significantly decreases, further stressing the careful design of nanostructure geometry to optimize F_V in relation to k_{e2} , as well as k_2 as previously discussed. Unsurprisingly, R_I is proportional to k_{e2} as well as F_V when $m = 1$, further supporting the claim that a concentration gradient is established. A similar trend is observed for R_I when $m = 2$ (Supplementary Figure 5B).

R_I and TOF are also explored as functions of F_V and k_1 for $m = 1, 2$ in Supplementary Figures 1 and 2 in order to assess the effect of $Cat - A$ formation. Both R_I and TOF increase exponentially with k_1 , R_I increases with F_V and TOF decreases with F_V as expected. Though worthy of noting, the model predicts TOF approaches appreciable values nearing 10^2 s^{-1} with a high k_1 ($>10^4 \text{ M}^{-m} \text{ s}^{-1}$), supporting the claim that low TOF observed in Figures 4 and 5C.

However, an unexpected result was obtained R_I and TOF were plotted as functions of F_V and k_{e1} (Supplementary Figures 3 and 4). In the $m = 1$ case, k_{e1} has little to no effect on R_I and TOF, and R_I increases with F_V and TOF decreases with F_V , as discussed previously. For $m = 2$, the model predicts an extremely drastic increase in both R_I and TOF once k_{e1} becomes greater than F_V , presumably because they have an exponential dependence on Cat . They are both proportional to F_V at low k_{e1} , but they are inversely proportional to F_V at high k_{e1} . We suspect that this is due to diffusion of Cat effectively out competing elimination when k_{e1} is low, leading to increased $Cat - A$ production and subsequently higher R_I and TOF. However, at high k_{e1} , elimination outcompetes Cat influx, elimination establishes a significant concentration gradient and any Cat already inside the compartment will outflux at rates proportional to F_V . Therefore, less $Cat - A$ will be produced and R_I and TOF decrease. Though mechanistically we are unable to account for the general increases in R_I and TOF with increasing k_{e1} from the perspective of Cat concentration, diffusion and conversion to $Cat - A$, as we expect k_{e1} to decrease R_I and TOF for both $m = 1, 2$.

Adapting the model to other nanostructures

Changing the theoretical framework established herein to fit varying organometallic catalytic cycles is relatively straightforward. The only anticipated issue would be knowing all relevant kinetic parameters. However, certain steps such as eliminations may be omitted or assumed to be infinitely fast to simplify the mathematical derivations. Adapting the framework to suit any nanostructure geometry is somewhat non-trivial. The derivation of F_V (or simply F) rests entirely on the definition of a compartment created by a particular nanostructure. Once a compartment is adequately defined, solving for F_V for the most part simply based on geometry. One other uncertainty is diffusion path/compartment thickness Δx . The definition of a compartment and Δx will be the focal point of this section.

In our previous report examining a solution catalytic cycle of incompatible steps with a nanowire array electrode as a compartmentalized system, we take the anaerobic domain established roughly half way down the wire as the compartment. Therefore we solve for the compartment boundary in terms of nanowire length (L), and define Δx as $0.5*L$, as a molecule outside of the nanowire array would half to travel half of the wire length to enter the compartment. In this case, Δx is more or less a diffusion path travelled to enter the compartment rather than a compartment thickness. However, in the example of MOF or carbon shell confinement, a more definitive compartment thickness may be defined that a molecule needs to diffuse through to enter

the compartment.^{4,22,23} From there, the surface area or volume of the compartment may be solved geometrically, provided sufficient characterization of the compartment.

CONCLUSION

Here we have developed a theoretical framework for compartmentalizing organometallic catalytic cycles by means of nanostructure confinement, using a generic three step cycle and a nanowire array generated anaerobic domain as an exemplary compartment. Through defining the anaerobic compartment geometrically, an expression for $F_V = F/VN_A$, where F is diffusive conductance, was generated as a function of nanowire length (L). We show that key reaction metrics, derived from solving for steady state concentrations of catalytic species in the compartment, are significantly enhanced under the same kinetic parameters when compartmentalized, versus a homogenous counterpart. Furthermore, we demonstrate that careful design of a nanostructure to produce an optimal F_V value in relation to kinetic parameters is a viable approach to optimization by plotting key reaction metrics as functions of F_V and k_n or k_{en} . Lastly, we discuss how the model may be adapted to suit other nanostructure geometries, where rigorous definition of the nanostructure generated compartment will be instrumental. The results from this study will assist in the a priori design of compartmentalized organometallics.

ASSOCIATE CONTENT

Supporting Information

Author Information

C. L. supervised the project. B. J. J. performed the mathematical derivations for the theoretical framework. All the authors discussed the results and assisted during the manuscript preparation.

Corresponding Author

*Email: chongliu@chem.ucla.edu

ORCID

Brandon J. Jolly: 0000-0003-4991-5212

Chong Liu: 0000-0001-5546-3852

Notes

The authors declare no competing financial interest.

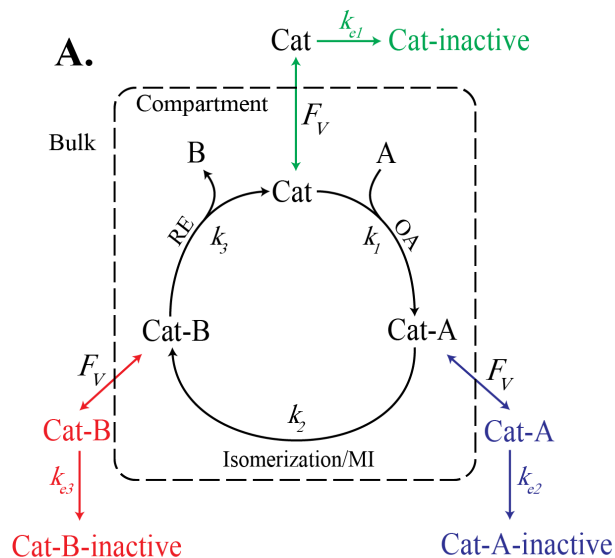
ACKNOWLEDGEMENTS

C. L. acknowledges the NSF Award (CHE-2027330), startup fund from the University of California, Los Angeles, and the financial support of the Jeffery and Helo Zink Endowed Professional Development Term Chair.

REFERENCES

1. Hurtley, S. (2009). Location, Location, Location. *Science*, 326(5957), 1205.

2. Jandt, U., You, C., Zhang, Y. H. P., & Zeng, A. P. (2013). Compartmentalization and Metabolic Channeling for Multienzymatic Biosynthesis: Practical Strategies and Modeling Approaches. In (pp. 41-65): Springer Berlin Heidelberg.
3. Chen, A. H., & Silver, P. A. (2012). Designing biological compartmentalization. *Trends in Cell Biology*, 22(12), 662-670.
4. Vázquez-González, M., Wang, C., & Willner, I. (2020). Biocatalytic cascades operating on macromolecular scaffolds and in confined environments. *Nature Catalysis*, 3(3), 256-273.
5. Hinzpeter, F., Gerland, U., & Tostevin, F. (2017). Optimal Compartmentalization Strategies for Metabolic Microcompartments. *Biophysical Journal*, 112(4), 767-779.
6. Zhang, Y., & Hess, H. (2017). Toward Rational Design of High-efficiency Enzyme Cascades. *ACS Catalysis*, 7(9), 6018-6027.
7. Chavan, K. S., & Calabrese Barton, S. (2018). Simulation of Intermediate Channeling by Nanoscale Confinement. *The Journal of Physical Chemistry C*.
8. Tsitkov, S., & Hess, H. (2019). Design Principles for a Compartmentalized Enzyme Cascade Reaction. *ACS Catalysis*, 9(3), 2432-2439.
9. Wayland, B. B., Ba, S., & Sherry, A. E. (1991). Activation of methane and toluene by rhodium(II) porphyrin complexes. *Journal of the American Chemical Society*, 113(14), 5305-5311.
10. Natinsky, B. S., Lu, S., Copeland, E. D., Quintana, J. C., & Liu, C. (2019). Solution Catalytic Cycle of Incompatible Steps for Ambient Air Oxidation of Methane to Methanol. *ACS Central Science*.
11. Natinsky, B. S., Jolly, B.J., Dumas, D. M., Liu, C. (2020) *ChemRxiv*
12. Pregosin, P. S., Kumar, P. A., & Fernández, I. (2005). *Chemical reviews*, 105(8), 2977-2998.
13. Drago, D., Pregosin, P. S., & Pfaltz, A. (2002). *Chemical Communications*(3), 286-287.
14. Ellis, P. R., Pearson, J. M., Haynes, A., Adams, H., Bailey, N. A., & Maitlis, P. M. (1994). *13*(8), 3215-3226.
15. Espenson, J. H., Pestovsky, O., Huston, P., & Staudt, S. (1994). *116*(7), 2869-2877.
16. Ju, T. D., Lang, R. F., Roper, G. C., & Hoff, C. D. (1996). *Journal of the American Chemical Society*, 118(22), 5328-5329.
17. Massick, S. M., & Ford, P. C. (1999). *Organometallics*, 18(21), 4362-4366.
18. Ford, P. C., & Massick, S. (2002). *Coordination chemistry reviews*, 226(1-2), 39-49.
19. Bochmann, M. (2004). *689*(24), 3982-3998
20. Breno, K. L., Pluth, M. D., Landorf, C. W., & Tyler, D. R. (2004). *Organometallics*, 23(8), 1738-1746.
21. Heiden, Z. M., & Rauchfuss, T. B. (2007). *129*(46), 14303-14310.
22. Liu, N., Lu, Z., Zhao, J., McDowell, M. T., Lee, H.-W., Zhao, W., & Cui, Y. (2014). A pomegranate-inspired nanoscale design for large-volume-change lithium battery anodes. *Nature Nanotechnology*, 9(3), 187-192.
23. Mohite, S. V., Xing, R., Li, B., Latthe, S. S., Zhao, Y., Li, X., . . . Liu, S. (2020). Spatial Compartmentalization of Cobalt Phosphide in P-Doped Dual Carbon Shells for Efficient Alkaline Overall Water Splitting. *Inorganic Chemistry*, 59(3), 1996-2004.



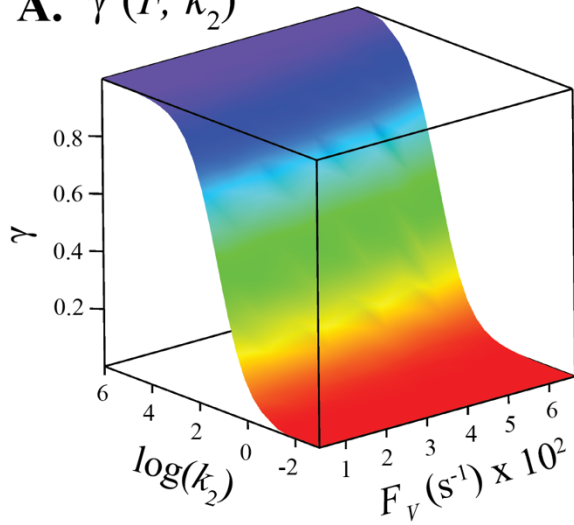
B. Key Reaction Metrics

<u>Compartmentalized</u>	<u>Non-Compartmentalized</u>
$R_S = k_1[\text{Cat}]$	$R_S = k_1[\text{Cat}]_0$
$R_I = F_V([\text{Cat-A}] - [\text{Cat-A}]_b)$	$R_I = k_{e2}[\text{Cat-A}]$
$R_P = k_3[\text{Cat-B}]$	$R_P = k_3[\text{Cat-B}]$
$\gamma = R_P/R_S$	$\gamma = R_P/R_S$
$\text{TOF} = R_P/[\text{Cat}]_0$	$\text{TOF} = R_P/[\text{Cat}]_0$

R_S (M s^{-1}) - substrate consumption
 R_I (M s^{-1}) - intermediate outflux/elimination
 R_P (M s^{-1}) - product formation
 γ - reaction efficiency
 TOF (s^{-1}) - turnover frequency
 F_V (s^{-1}) = F/VN_A F (M s^{-1}) - diffusive conductance

Figure 1. General compartmentalized catalytic cycle (**A**) used to construct the mathematical model and key reaction metrics (**B**) used to compare the compartmentalized framework to an analogous homogeneous (non-compartmentalized).

A. $\gamma(F, k_2)$



B. $\gamma(k_2)$

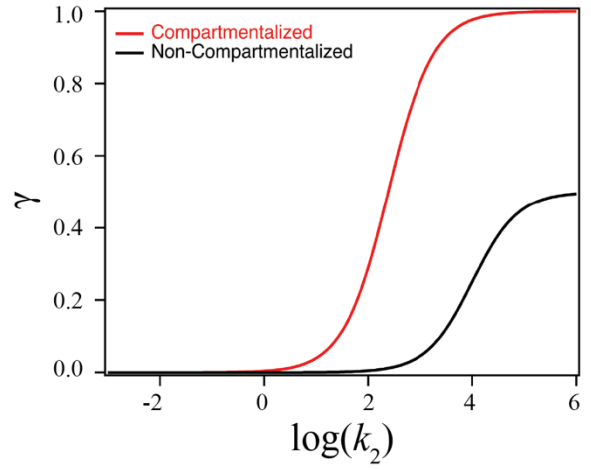


Figure 2. Compartmentalized γ as a function of F_V and $\log(k_2)$ (**A**) and comparison between compartmentalized (at $F_V = 320 \text{ s}^{-1}$ for a $15 \mu\text{m}$ example wire array) and non-compartmentalized γ (**B**), both at $k_{e2} = 1 \times 10^3 \text{ s}^{-1}$ and $k_3 = k_{e3} = 1 \times 10^6 \text{ s}^{-1}$.

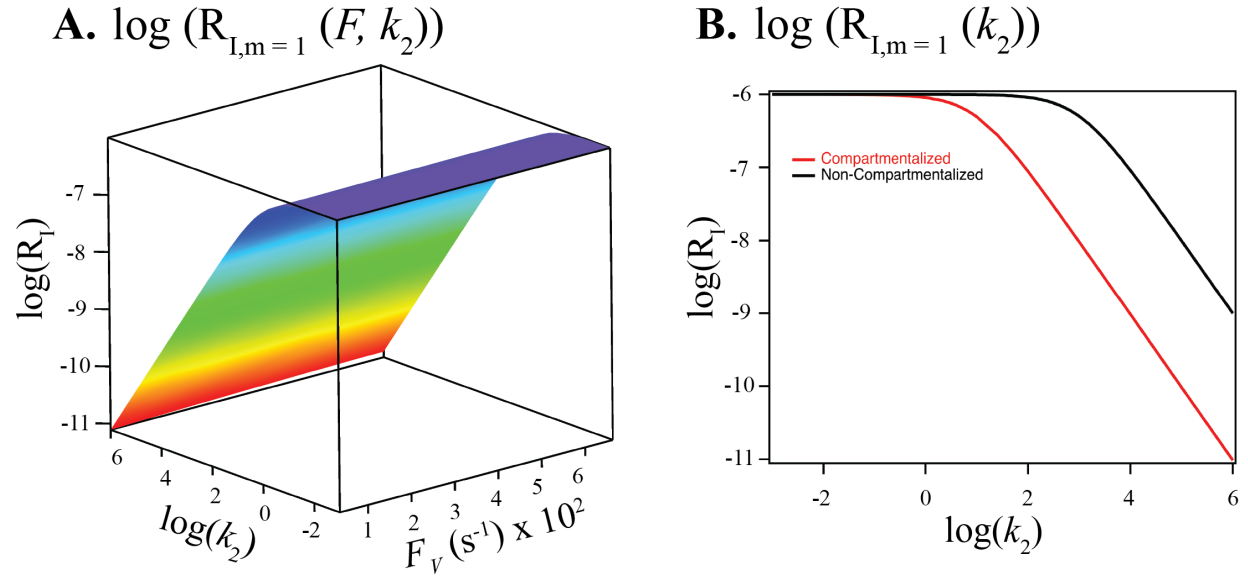
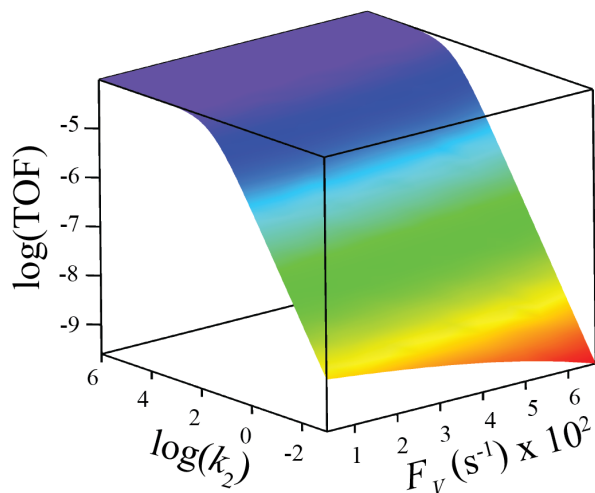


Figure 3. Compartmentalized $R_{I,m=1}$ as a function of F_V and $\log(k_2)$ (A) and comparison between compartmentalized (at $F_V = 320 \text{ s}^{-1}$ for a $15 \mu\text{m}$ example wire array) and non-compartmentalized $R_{I,m=1}$ (B), both at $k_1 = k_{e1} = 0.1 \text{ M}^{-1} \text{ s}^{-1}$, $k_{e2} = 1 \times 10^3 \text{ s}^{-1}$, and $k_3 = k_{e3} = 1 \times 10^6 \text{ s}^{-1}$.

A. $\log(\text{TOF}_{m=1}(F, k_2))$



B. $\log(\text{TOF}_{m=1}(k_2))$

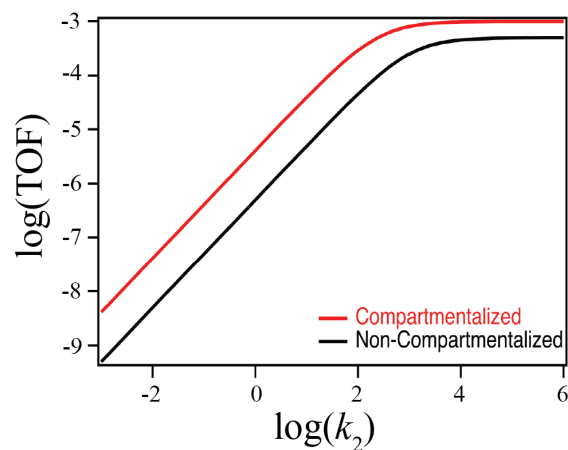


Figure 4. Compartmentalized $\text{TOF}_{m=1}$ as a function of F_V and $\log(k_2)$ (**A**) and comparison between compartmentalized (at $F_V = 320 \text{ s}^{-1}$ for a $15 \mu\text{m}$ example wire array) and non-compartmentalized $\text{TOF}_{m=1}$ (**B**), both at $k_1 = k_{e1} = 0.1 \text{ M}^{-1} \text{ s}^{-1}$, $k_{e2} = 1 \times 10^3 \text{ s}^{-1}$, and $k_3 = k_{e3} = 1 \times 10^6 \text{ s}^{-1}$.

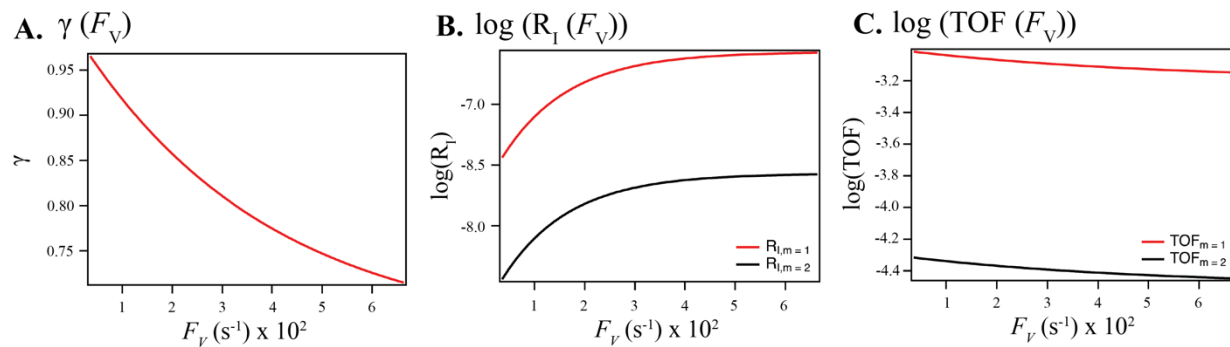


Figure 5. Compartmentalized γ (A), R_I (B), and TOF (C) as a function of F_V all at $k_1 = k_{e1} = 0.1 \text{ M}^{-1} \text{ s}^{-1}$ ($m = 1$) or $10 \text{ M}^{-2} \text{ s}^{-1}$ ($m = 2$), $k_2 = k_{e2} = 1 \times 10^3 \text{ s}^{-1}$, and $k_3 = k_{e3} = 1 \times 10^6 \text{ s}^{-1}$.

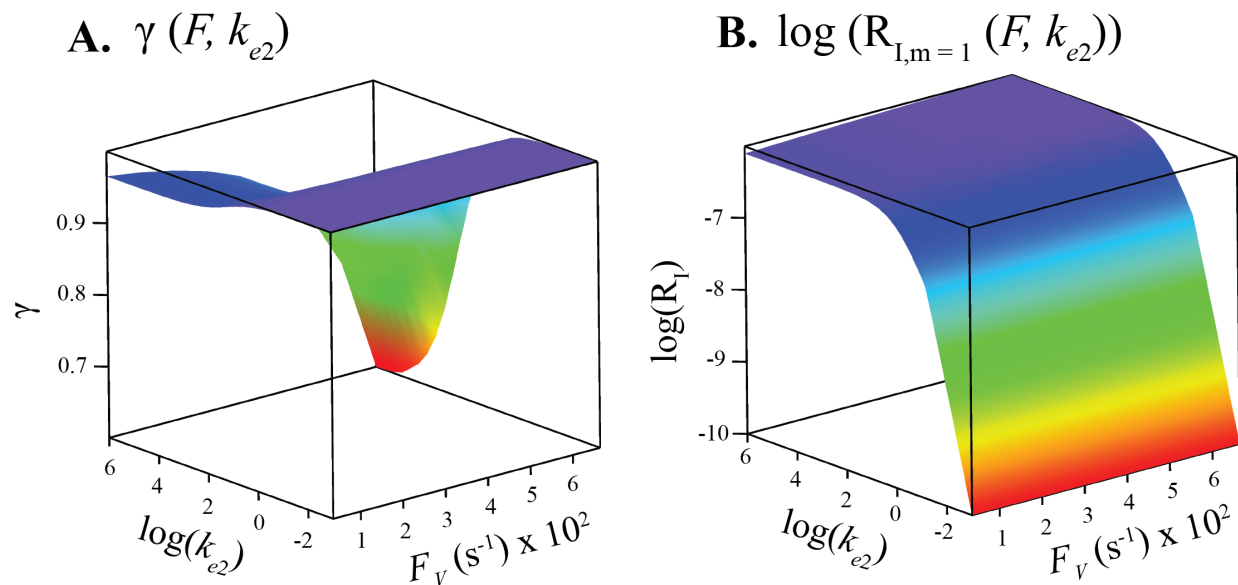


Figure 6. Compartmentalized γ (**A**) and $R_{I,m=1}$ (**B**) as a function of F_V and $\log(k_{e2})$, both at $k_1 = k_{e1} = 0.1 \text{ M}^{-1} \text{ s}^{-1}$, $k_2 = 1 \times 10^3 \text{ s}^{-1}$, and $k_3 = k_{e3} = 1 \times 10^6 \text{ s}^{-1}$.